Set-Valued Approach for the Online Identification of the Open-Circuit Voltage of Lithium-Ion Batteries

Marit Lahme[ab] and Andreas Rauh[ac]

Abstract

To describe the dynamic behavior of lithium-ion batteries using the terminal current and the terminal voltage as input and output of the battery, equivalent circuit models are used, which comprise series resistances, RC subnetworks and a state of charge dependent voltage source. The parameters of the battery model are influenced by aging effects as well as other factors such as the state of charge and the cell temperature. Although those variations can be estimated with the help of an augmented state vector, the typically applied approaches do not allow for a direct identification of nonlinear dependencies of circuit elements on the state of charge or other influence factors. Therefore, a two-stage identification routine for identifying those nonlinear dependencies using an interval observer and an interval contraction scheme is proposed in this paper. The identification routine was successfully applied to identify the open-circuit voltage characteristic of a lithium-ion battery. Numerical simulations are used to evaluate the identification quality of the identification routine.

Keywords: online identification, interval methods, lithium-ion batteries

1 Introduction

The charging/discharging dynamics of lithium-ion batteries can be approximated by using equivalent circuit models. According to [4, 7, 15], these models consist of a finite number of RC sub-networks as well as series resistances and a state of charge (SOC) dependent voltage source which represents the open-circuit voltage. In classical state estimation approaches, the parameters are identified beforehand (cf. [4, 7, 15]). However, the parameters of battery models are subject to aging and temperature induced variations, which is shown in [4]. The aging of battery cells leads to a loss of the total capacity, an increasing Ohmic cell resistance and changes in the charging/discharging efficiency as well as changes of the delay parameters of the aforementioned RC sub-networks. Additionally, many degradation mechanisms

[a]Carl von Ossietzky Universität Oldenburg, Distributed Control in Interconnected Systems
[b]E-mail: marit.lahme@uni-oldenburg.de, ORCID: 0000-0001-8633-1908
[c]E-mail: andreas.rauh@uni-oldenburg.de, ORCID: 0000-0002-1548-6547

of lithium-ion batteries that lead to capacity or power fading are highly dependent on the cell temperature [3]. Many of these parameter variations can be mapped onto the open-circuit voltage and estimated during system operation with the help of an augmented state vector, but this approach does not allow for estimating nonlinear functional dependencies of the circuit elements on the SOC or other influence factors. The above-mentioned variations can alternatively be detected offline using electrochemical impedance spectroscopy (EIS), as mentioned in [1, 12, 13]. The EIS method is to apply a sinusoidal current (sinusoidal voltage) to the battery over a wide frequency range and to measure the terminal voltage (terminal current). The spectroscopic features of the resulting impedance spectrum can be assigned to the components of the corresponding equivalent circuit model. The impedance is affected by a variety of factors such as the cell temperature, aging, or the SOC. Accordingly, variations resulting from these influence factors can be detected using EIS. The drawback of this method is that it takes a long time typically in the range of hours to days because of the gradual charging/discharging process and resting periods that might be necessary.

To address these difficulties, we propose a two-stage identification of nonlinear dependencies in this paper with the dependency of the open-circuit voltage on the SOC as an example. This two-stage identification is based on interval analysis, which has already been used successfully in parameter estimation, for example in [2]. Therefore, it is a promising method for this online identification routine. The state variables of the dynamic system are estimated in the first stage with an interval observer. In the second stage, the a-priori knowledge of the open-circuit voltage characteristic is corrected using the estimated state variables. For the identification of the nonlinear dependency of the open-circuit voltage on the SOC with underlying aging and temperature induced variations, it is assumed that the other equivalent circuit parameters are known and not yet affected by aging.

This paper is structured as follows. Section 2 outlines the modeling of lithium-ion batteries based on equivalent circuit models. In Section 3, the design of the interval observer is described which is used for the identification routine shown in Section 4. The results of the numerical simulation for evaluating the performance of this set-valued identification approach are presented in Section 5. The paper is concluded with a brief summary of the proposed identification routine as well as with an outlook on future work in Section 6.

Notation. In this paper, matrices and vectors are denoted by bold letters to distinguish them from scalar variables. The notations $\underline{\mathbf{M}}$ and $\overline{\mathbf{M}}$ for an interval matrix $\mathbf{M}$ denote the element-wise lower and upper bounds.

2   Equivalent Circuit Model of Lithium-Ion Batteries

In this paper, an equivalent circuit model containing one series resistance and two RC sub-networks representing processes with short (τ_{TS}) and large (τ_{TL}) time con-

stants resulting from polarization effects and concentration losses is considered as shown in Fig. 1 [4, 15]. Here, v_{OC} is the open-circuit voltage. The terminal current i_{T} is used as the input to charge or discharge the battery and the terminal voltage v_{T} can be measured. The instantaneous voltage drop of the terminal voltage is caused by the serial resistance R_{S}. The two RC sub-networks consisting of C_{TS}, C_{TL}, R_{TS}, and R_{TL} are used to describe the transient behavior. First, the modeling of lithium-ion batteries is introduced with point-valued state variables and crisp equivalent circuit parameters. At the end of this section, the model is extended to interval values.
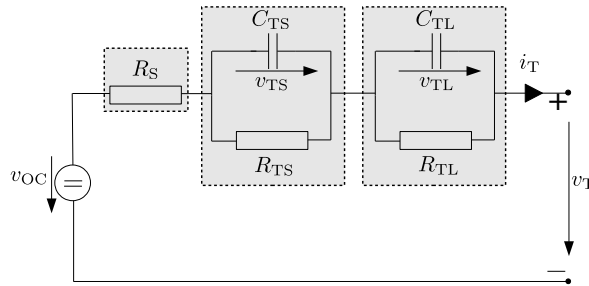

Figure 1: Equivalent circuit model of a lithium-ion battery (modified from [15]).

The SOC $\sigma(t)$ and the voltages across the RC sub-networks $v_{\text{TS}}(t)$ and $v_{\text{TL}}(t)$ are chosen as the state variables. Hence, the state vector

$$\mathbf{x}(t) = \begin{bmatrix} \sigma(t) & v_{\text{TS}}(t) & v_{\text{TL}}(t) \end{bmatrix}^T \tag{1}$$

and the quasi-linear, continuous time state equations

$$\dot{\mathbf{x}}(t) = \mathbf{A}\left(\sigma(t)\right) \cdot \mathbf{x}(t) + \mathbf{b}\left(\sigma(t)\right) \cdot u(t) \tag{2}$$

$$= \begin{bmatrix} 0 & 0 & 0 \\ 0 & \frac{-1}{C_{\text{TS}}(\sigma(t)) \cdot R_{\text{TS}}(\sigma(t))} & 0 \\ 0 & 0 & \frac{-1}{C_{\text{TL}}(\sigma(t)) \cdot R_{\text{TL}}(\sigma(t))} \end{bmatrix} \cdot \mathbf{x}(t) + \begin{bmatrix} \frac{-1}{C_{\text{Bat}}} \\ \frac{1}{C_{\text{TS}}(\sigma(t))} \\ \frac{1}{C_{\text{TL}}(\sigma(t))} \end{bmatrix} \cdot u(t)$$

are obtained, where the system input is given as the terminal current $u(t) := i_{\text{T}}(t)$. The SOC as well as $v_{\text{TS}}(t)$ and $v_{\text{TL}}(t)$ can be point-valued or interval values. The first state equation represents the integrating behavior

$$\dot{\sigma}(t) = -\frac{i_{\text{T}}(t)}{C_{\text{Bat}}} \tag{3}$$

between the SOC $\sigma(t) \in [0\,;\,1]$ and the charging/discharging current $i_{\text{T}}(t)$. Here, the SOC is a normalized value, so that $\sigma = 0$ corresponds to the completely discharged battery and $\sigma = 1$ represents the fully charged battery with the nominal

capacitance C_{Bat}. The other two state equations represent the first-order lag behavior of the RC sub-networks

$$\dot{v}_\iota(t) = \frac{-v_\iota(t)}{C_\iota(\sigma(t)) \cdot R_\iota(\sigma(t))} + \frac{i_{\mathrm{T}}(t)}{C_\iota(\sigma(t))} \ , \quad \iota \in \{\mathrm{TS}, \mathrm{TL}\} \tag{4}$$

where the equivalent circuit parameters and the delay parameters are dependent on the SOC according to

$$R_\iota(\sigma(t)) = R_{\iota\mathrm{a}} \cdot e^{R_{\iota\mathrm{b}} \cdot \sigma(t)} + R_{\iota\mathrm{c}} \ , \quad \iota \in \{\mathrm{TS}, \mathrm{TL}\} \ , \tag{5}$$

$$C_\iota(\sigma(t)) = C_{\iota\mathrm{a}} \cdot e^{C_{\iota\mathrm{b}} \cdot \sigma(t)} + C_{\iota\mathrm{c}} \ , \quad \iota \in \{\mathrm{TS}, \mathrm{TL}\} \ , \tag{6}$$

$$\tau_\iota(\sigma(t)) = C_\iota(\sigma(t)) \cdot R_\iota(\sigma(t)) \ , \quad \iota \in \{\mathrm{TS}, \mathrm{TL}\} \ . \tag{7}$$

The SOC-dependent parameters have been identified in [17] using experimental parameter identification. The identified parameters are shown in Tab. 1. By applying Kirchhoff's voltage law, the terminal voltage is obtained as

$$v_{\mathrm{T}}(t) = v_{\mathrm{OC}}(\sigma(t)) - v_{\mathrm{TS}}(t) - v_{\mathrm{TL}}(t) - i_{\mathrm{T}}(t) \cdot R_{\mathrm{S}}(\sigma(t)) \ , \tag{8}$$

with the Ohmic resistance

$$R_{\mathrm{S}}(\sigma(t)) = R_{\mathrm{Sa}} \cdot e^{R_{\mathrm{Sb}} \cdot \sigma(t)} + R_{\mathrm{Sc}} \ . \tag{9}$$

Based on the experimental parameter identification in [17], the open-circuit voltage is assumed to be represented by the nonlinear expression

$$v_{\mathrm{OC}}(\sigma(t)) = v_0 \cdot e^{v_1 \cdot \sigma(t)} + \sum_{i=0}^{3} v_{i+2} \cdot \sigma^i(t) \ , \tag{10}$$

which can be rewritten in the quasi-linear form

$$\tilde{v}_{\mathrm{OC}}(\sigma(t)) = \eta_{\mathrm{OC}}(\sigma(t)) \cdot \sigma(t) = v_{\mathrm{OC}}(\sigma(t)) - v_0 - v_2 \tag{11}$$

$$= \left(v_0 \cdot \frac{e^{v_1 \cdot \sigma(t)} - 1}{\sigma(t)} + v_3 + v_4 \cdot \sigma(t) + v_5 \cdot \sigma^2(t) \right) \cdot \sigma(t) \tag{12}$$

by subtracting the constant, state-independent terms from the expression for the open-circuit voltage [15]. Using (8) and (12), the output equation can be obtained as

$$y(t) = \tilde{v}_{\mathrm{T}}(t) = \mathbf{C}(\sigma(t)) \cdot \mathbf{x}(t) + \mathbf{D}(\sigma(t)) \cdot i_{\mathrm{T}}(t) \tag{13}$$
$$= \tilde{v}_{\mathrm{OC}}(t) - v_{\mathrm{TS}}(t) - v_{\mathrm{TL}}(t) - i_{\mathrm{T}}(t) \cdot R_{\mathrm{S}}(t) \ ,$$

and can be rewritten in the quasi-linear input-independent form

$$y^*(t) = y(t) - \mathbf{D}(\sigma(t)) \cdot i_{\mathrm{T}}(t) = \mathbf{C}(\sigma(t)) \cdot \mathbf{x}(t) \tag{14}$$
$$= \begin{bmatrix} \eta_{\mathrm{OC}}(\sigma(t)) & -1 & -1 \end{bmatrix} \cdot \mathbf{x}(t) \in [y_{\mathrm{m}}] \ ,$$

with the output matrix $\mathbf{C}\left(\sigma(t)\right) = \begin{bmatrix} \eta_{\mathrm{OC}}\left(\sigma(t)\right) & -1 & -1 \end{bmatrix}$ (which is a row vector in the special case of this paper) and the feedthrough matrix $\mathbf{D}\left(\sigma(t)\right) = -R_{\mathrm{S}}(\sigma(t))$. In (14), $\mathrm{y}^*(t)$ represents the measurement that is provided to the observer. It is the terminal voltage of the battery, adjusted in a way that it is expressed according to the quasi-linear output equation. Furthermore, the measurement noise (assumed to be bounded) has to be considered, so that $\mathrm{y}^*(t)$ is an element of the measurement interval $[\mathrm{y_m}]$, defined in (22). Outliers, for example measurements that are wrong, may affect the estimation quality of the interval observer designed in Section 3 and therefore may also affect the identification quality of the open-circuit voltage characteristic. In this paper, we assume that there are no outliers, but managing outliers can be done in future work with applying relaxed set inversion techniques as shown in [2] and [8].

To implement the proposed identification approach, the continuous time system is temporally discretized with a constant step size T and approximated with the help of the explicit Euler method. Because of the small sampling time T compared to the delay parameters τ_{TS} and τ_{TL}, this method is sufficiently accurate. The discretization errors are assumed to be included in the measurement uncertainty. With $\mathbf{x}_k$ and σ_k approximating the exact state values $\mathbf{x}(t_k)$ and $\sigma(t_k)$ in the discretization points, the discretized state equations are then obtained as

$$\mathbf{x}_{k+1} = \mathbf{A}_{\mathrm{d}}\left(\sigma_k\right) \cdot \mathbf{x}_k + \mathbf{b}_{\mathrm{d}}\left(\sigma_k\right) \cdot u_k \ , \tag{15}$$

$$\mathbf{A}_{\mathrm{d}}\left(\sigma_k\right) = \mathbf{I}_{3\times3} + T \cdot \mathbf{A}\left(\sigma_k\right) \ , \tag{16}$$

$$\mathbf{b}_{\mathrm{d}}\left(\sigma_k\right) \cdot u_k = T \cdot \mathbf{b}\left(\sigma_k\right) \cdot u_k \ . \tag{17}$$

In this paper, interval state variables are considered, so that $\mathbf{x}(t) \in [\underline{\mathbf{x}}(t) \ ; \ \overline{\mathbf{x}}(t)]$ is a vector consisting of intervals for each component. Therefore, also the equivalent circuit parameters become intervals, which leads to interval-valued matrices $\mathbf{A}\left(\sigma(t)\right) \in \left[\underline{\mathbf{A}}\left(\sigma(t)\right) \ ; \ \overline{\mathbf{A}}\left(\sigma(t)\right)\right]$, $\mathbf{b}\left(\sigma(t)\right) \in \left[\underline{\mathbf{b}}\left(\sigma(t)\right) \ ; \ \overline{\mathbf{b}}\left(\sigma(t)\right)\right]$, $\mathbf{C}\left(\sigma(t)\right) \in \left[\underline{\mathbf{C}}\left(\sigma(t)\right) \ ; \ \overline{\mathbf{C}}\left(\sigma(t)\right)\right]$ and $\mathbf{D}\left(\sigma(t)\right) \in \left[\underline{\mathbf{D}}\left(\sigma(t)\right) \ ; \ \overline{\mathbf{D}}\left(\sigma(t)\right)\right]$. This also applies to the discretized system.

3 Design of the Interval Observer

The proposed identification approach for nonlinear dependencies of the circuit elements on state variables is a two-stage procedure. In the first stage, state estimation is performed with an interval observer in each time step. Therefore, the most recent estimate for the state vector is used which consists of intervals for each component. The estimated values are then used in the second stage to correct the a-priori knowledge for the open-circuit voltage characteristic. The estimation of the state variables and the open-circuit voltage is shown in Fig. 2.

A prerequisite for this identification approach is that all state variables can be estimated. Hence, the system has to be observable or identifiable. The observer gain matrix $\mathbf{H}$ is designed in such a way that the stability is ensured for the assumed open-circuit voltage characteristic. The system matrix $\mathbf{A}\left(\sigma(t)\right)$ from equation (2) has the following sign pattern
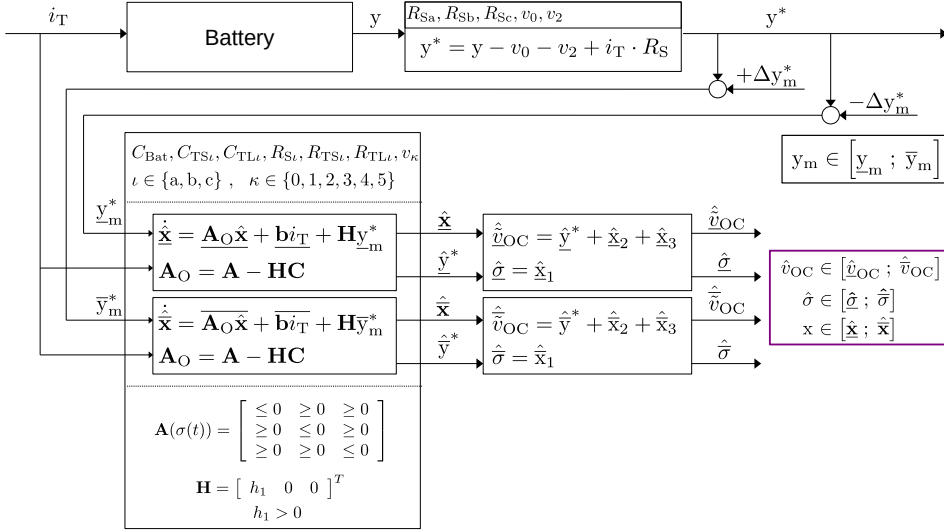
Figure 2: Estimation of the open-circuit voltage and the state of charge.

$$\mathbf{A}\left(\sigma(t)\right) = \begin{bmatrix} \leq 0 & \geq 0 & \geq 0 \\ \geq 0 & \leq 0 & \geq 0 \\ \geq 0 & \geq 0 & \leq 0 \end{bmatrix} \in \left[\underline{\mathbf{A}} \; ; \; \overline{\mathbf{A}}\right] . \tag{18}$$

Based on the design of a robust interval observer shown in [7], the observer matrix $\mathbf{H}$ is hereby assigned as

$$\mathbf{H} = \begin{bmatrix} h_1 & 0 & 0 \end{bmatrix}^T , \; h_1 > 0 , \tag{19}$$

where h_1 is a scalar.

With the bounding systems $\mathbf{x} \in [\underline{\mathbf{x}} \; ; \; \overline{\mathbf{x}}]$ for the true states and $\hat{\mathbf{x}} \in [\hat{\mathbf{x}}] := \left[\underline{\hat{\mathbf{x}}} \; ; \; \overline{\hat{\mathbf{x}}}\right]$ for their estimates, respectively, $\mathbf{x}$ is given as $\mathbf{x} \in \left[\underline{\hat{\mathbf{x}}} \; ; \; \overline{\hat{\mathbf{x}}}\right]$ and the interval observer is obtained according to [7] and [14] as

$$\underline{\mathbf{A}_O}\hat{\mathbf{x}} + \underline{\mathbf{b}\mathbf{u}} + \mathbf{H}\underline{\mathbf{y}}_m \leq \dot{\hat{\mathbf{x}}} \leq \overline{\mathbf{A}_O\hat{\mathbf{x}}} + \overline{\mathbf{b}\mathbf{u}} + \mathbf{H}\overline{\mathbf{y}}_m \; , \; \hat{\mathbf{x}} \in [\hat{\mathbf{x}}] \tag{20}$$

with the observer system matrix

$$\mathbf{A}_O = \mathbf{A} - \mathbf{H}\mathbf{C} \in \left[\underline{\mathbf{A}}_O \; ; \; \overline{\mathbf{A}}_O\right] \tag{21}$$

and the uncertain measurements

$$[\mathbf{y}_m] := \left[\underline{\mathbf{y}}_m \; ; \; \overline{\mathbf{y}}_m\right] = \mathbf{y}_m + \left[-\Delta\mathbf{y}_m \; ; \; \Delta\mathbf{y}_m\right] . \tag{22}$$

The observer is parameterized in a cooperativity preserving way [6, 9]. Cooperative dynamic systems have state trajectories that are monotonic with respect to

the initial conditions. Lower and upper bounds for the states of uncertain cooperative systems can be calculated by solving two independent initial value problems, one for each bound. Hence, the computational effort to determine these lower and upper bounds is reduced in comparison to a non-cooperative model. A system

$$\dot{\mathbf{x}}(t) = \mathbf{f}(\mathbf{x}(t)), \ \ \mathbf{x} \in \mathbb{R}^n, \tag{23}$$

has to fulfill the following two conditions to be cooperative. All off-diagonal elements of its Jacobian

$$\mathbf{J} = \frac{\partial \mathbf{f}(\mathbf{x})}{\partial \mathbf{x}} \tag{24}$$

have to be non-negative

$$J_{i,j} \geq 0, \ \ i,j \in \{1, ..., n\}, \ \ i \neq j \tag{25}$$

and all state variables have to be non-negative [6, 9]

$$\mathbf{x} \in \mathbb{R}_{\geq 0} \ . \tag{26}$$

Due to the design of the observer gain matrix, the observer system matrix $\mathbf{A}_{\mathrm{O}}$ and the system matrix $\mathbf{A}$ have the same sign pattern. Therefore, adding this interval observer to a cooperative system preserves the property of cooperativity.

For cooperative systems, guaranteed state enclosures are found by considering $\underline{\mathbf{A}}_{\mathrm{O}}\hat{\underline{\mathbf{x}}}$ and $\overline{\mathbf{A}}_{\mathrm{O}}\hat{\overline{\mathbf{x}}}$ for the lower and upper bound respectively in equation (20), if all state variables are element wise non-negative. The system in equation (2), however, does not satisfy the conditions (25) and (26). Hence, it is not cooperative in this simplest form [6]. Therefore, guaranteed lower and upper bounds for all state variables of the system (2) have to be calculated according to Müller's theorem [5], without taking advantage of the property of cooperativity. This is done by considering the infimum (supremum) of $\mathbf{A}_{\mathrm{O}}\hat{\mathbf{x}}$ for the lower bound (upper bound) in equation (20).

Like the continuous time system (2), the observer is also discretized with a constant step size T and with the help of the explicit Euler method. This leads to the following equations:

$$\hat{\mathbf{x}}_{k+1} = \mathbf{A}_{\mathrm{Od}}\left(\hat{\sigma}_k\right) \cdot \hat{\mathbf{x}}_k + \mathbf{b}_{\mathrm{d}}\left(\hat{\sigma}_k\right) \cdot u_k + \mathbf{H}_{\mathrm{d}} \cdot \mathrm{y}_{\mathrm{m},k} \ , \tag{27}$$

$$\mathbf{A}_{\mathrm{Od}}\left(\hat{\sigma}_k\right) = \mathbf{I}_{3 \times 3} + T \cdot \mathbf{A}_{\mathrm{O}}\left(\hat{\sigma}_k\right) \ , \tag{28}$$

$$\mathbf{b}_{\mathrm{d}}\left(\hat{\sigma}_k\right) \cdot u_k = T \cdot \mathbf{b}\left(\hat{\sigma}_k\right) \cdot u_k \ , \tag{29}$$

$$\mathbf{H}_{\mathrm{d}} \cdot \mathrm{y}_{\mathrm{m},k} = T \cdot \mathbf{H} \cdot \mathrm{y}_{\mathrm{m},k} \ . \tag{30}$$

In order to guarantee stability for the discretized observed system, the magnitudes of all eigenvalues of the matrix $\mathbf{A}_{\mathrm{Od}}$ have to be less than one. To preserve the derivation of lower and upper bounding systems, the system matrix in (28) needs to be element wise non-negative. The evaluation of this discretized model is performed in analogy to equation (17) in [16].

4   Identification of the open-circuit voltage

With the help of interval methods, the nonlinear dependency of the open-circuit voltage on the SOC can be identified as visualized in Fig. 3. During the charging/discharging process of the battery, the values of the open-circuit voltage and the state of charge are estimated by the interval observer resulting in axis-aligned interval boxes for the SOC and the open-circuit voltage. An interval box $[\mathbf{\Gamma}]$ is defined as the Cartesian product of closed intervals. Here, $[\mathbf{\Gamma}]$ is an element of $\mathbb{IR}^2$ and is defined as $[\mathbf{\Gamma}] = [\sigma(t)] \times [\tilde{v}_{\mathrm{OC}}(t)]$ with $\sigma(t) \in [\underline{\sigma}(t)\,;\,\overline{\sigma}(t)]$ and $\tilde{v}_{\mathrm{OC}}(t) \in [\underline{\tilde{v}}_{\mathrm{OC}}(t)\,;\,\overline{\tilde{v}}_{\mathrm{OC}}(t)]$. The open-circuit voltage is calculated based on the estimated state variables and equation (14)

$$\tilde{v}_{\mathrm{OC}}(t) = y_{\mathrm{m}}^*(t) + v_{\mathrm{TS}}(t) + v_{\mathrm{TL}}(t) \ . \tag{31}$$

The intersections of those interval boxes are utilized to improve the approximation of the true $v_{\mathrm{OC}}(\sigma(t))$ characteristic.
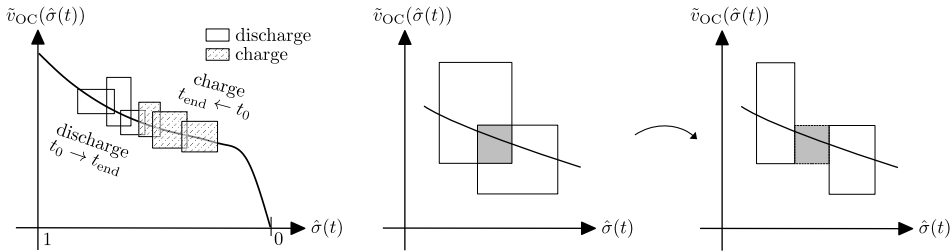
Figure 3: Identification of nonlinear dependencies using interval methods.

To keep the computational effort that is required for this intersection process feasible, merging strategies are necessary. A certain number of overlapping interval boxes are combined with the help of their convex interval hull as shown in Fig. 4. The resulting convex hulls are intersected with each other. The convex interval hull of two interval boxes $[\mathbf{\Gamma}_1]$ and $[\mathbf{\Gamma}_2]$ is denoted by

$$[\mathbf{\Gamma}_{\mathrm{hull}}] = [\mathbf{\Gamma}_1] \sqcup [\mathbf{\Gamma}_2] \ . \tag{32}$$

The overapproximation of two interval boxes with the convex interval hull results in an overestimation of the magnitude

$$\delta_{hull} = \frac{area\{[\mathbf{\Gamma}_{\mathrm{hull}}]\} - (area\{[\mathbf{\Gamma}_1]\} + area\{[\mathbf{\Gamma}_2]\}) + area\{[\mathbf{\Gamma}_1] \cap [\mathbf{\Gamma}_2]\}}{area\{[\mathbf{\Gamma}_1]\} + area\{[\mathbf{\Gamma}_2]\} - area\{[\mathbf{\Gamma}_1] \cap [\mathbf{\Gamma}_2]\}} \cdot 100\% \ ,$$

$$\tag{33}$$

where the area of an interval box is equal to the product of the interval widths of all components [10]. The overestimation for combining more than two interval boxes with the help of the corresponding convex interval hull can be calculated by

recursively applying equation (33), where δ_{hull} represents the exact overestimation, when two interval boxes are combined. Otherwise, it represents the upper bound on the overestimation. During the numerical simulation shown in this paper, the number of interval boxes that are approximated with the convex interval hull is defined beforehand. At the end of the simulation, the overestimation δ_{hull} is calculated for each convex interval hull.

Remark. Instead of using a preset, constant number of interval boxes that should be merged before the intersection process, a limit on the overestimation can be introduced. In this case, the interval boxes are recursively merged as long as the overestimation remains below the threshold $\delta_{hull} \leq \delta_{hull,max}$.
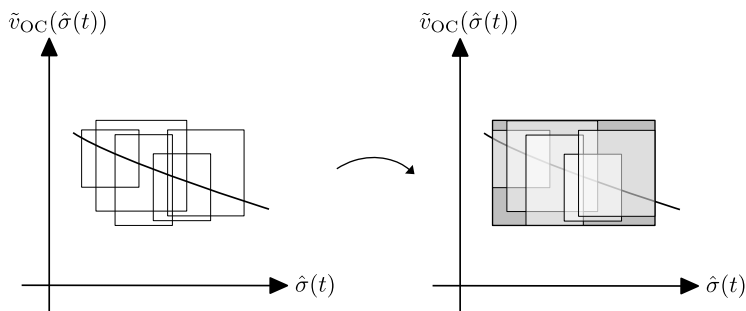
Figure 4: Combining interval boxes with the help of their convex interval hull.

5 Numerical Simulation

To evaluate the identification quality of the proposed identification routine, a numerical simulation was performed for the initial state $\mathbf{x}_0 = \begin{bmatrix} 0.9 & 0 & 0 \end{bmatrix}^T$ and the system parameters shown in Table 1. The discretization step size and the observer gain matrix are chosen as $T = 10\,\text{ms}$ and $\mathbf{H} = \begin{bmatrix} 0.2 & 0 & 0 \end{bmatrix}^T$. The magnitude of the bounded measurement noise is set to $\Delta y_m = 2.5\,\text{mV}$. The measurements are generated in a simulation using y and uniformly distributed random numbers in the interval of $[-\Delta y_m \, ; \, \Delta y_m]$. The input current has an amplitude of $5\,\text{A}$ and a period length of $1\,\text{h}$ and is given as shown in Fig. 5. To reduce the uncertainty and improve the estimation results, the input current consists of an alternating sequence of sine half-waves and periods where the current is constant and equal to zero. The number of interval boxes that are combined with the help of their convex interval hull is chosen as 6000. This corresponds to merging the interval boxes in a time span of one minute and leads to an overestimation of each interval hull of less than $3.73\,\%$. The true values are calculated based on point-valued state variables, point-valued equivalent circuit parameters and the system parameters shown in

Table 1: System parameters according to the experimental parameter identification in [17].

C_{Bat}	3.100	Ah	R_{TSa}	1	Ω	R_{TLa}	0.01	Ω	v_0	-1	V
			R_{TSb}	-30		R_{TLb}	-4		v_1	-23	
R_{Sa}	0.25	Ω	R_{TSc}	0.015	Ω	R_{TLc}	0.05	Ω	v_2	3.255	V
R_{Sb}	-20		C_{TSa}	-900	F	C_{TLa}	25000	F	v_3	0.8342	V
R_{Sc}	0.07	Ω	C_{TSb}	-2		C_{TLb}	-2		v_4	-0.2905	V
			C_{TSc}	1000	F	C_{TLc}	2000	F	v_5	0	V

Tab. 1. The simulation is implemented in MATLAB. The single core simulation of the interval observer and the intersection process is approximately four times faster than real time, so that this implementation is applicable for online identification purposes.

Figs. 6 and 7 show the estimation results for the three state variables. During the simulation, the estimation uncertainty increases but can be reduced by the periods of constant current, because the integrating behavior between the SOC and the terminal current is the main contribution to the uncertainty. It can only be reduced if the constant current is equal to zero. Otherwise, the uncertainty increases instead of being reduced. The uncertainty of the voltage v_{TS} decreases faster than the uncertainty of the voltage v_{TL} because of the smaller delay parameter τ_{TS} compared to the delay parameter τ_{TL}. The frequency of the input current also affects the estimation uncertainty. This is shown in Figs. 8 and 9. Here, the input currents $i_{\mathrm{T}}(t) = 5\,\mathrm{A} \cdot \sin\left(\frac{2\pi}{3600}t\right)$ and $i_{\mathrm{T}}(t) = 5\,\mathrm{A} \cdot \sin\left(\frac{10\pi}{3600}t\right)$ are compared. With increasing frequency, the estimation uncertainty decreases. However, the achievable SOC range also decreases, which in turn influences the identification process.

The identification result is shown in Fig. 10. Fig. 10(a) shows the identification result after the first sine half-wave of the input current (discharging process). It is obvious that the increasing uncertainty leads to an increasing width of the interval boxes. As mentioned before, the uncertainty is then reduced due to the constant current period so that, during the following charging process (second sine half-wave), the width of the interval boxes is further reduced (Fig. 10(b)). Here, the identification result of the discharging process serves as the a-priori knowledge for the characteristic to be identified. The true value of the $v_{\mathrm{OC}}(\sigma(t))$ characteristic can be approximated well in the range of the SOC that can be achieved during both discharging and charging processes.

6 Conclusions and Future Work

In this paper, a set-valued approach for the online identification of state-dependent characteristics was presented. This identification routine consists of two stages. At first, the state variables of the dynamic system are estimated with an interval
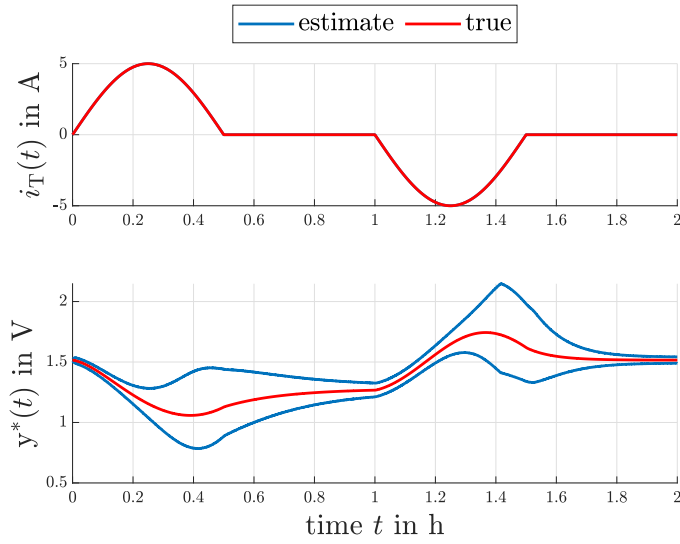
Figure 5: True output value $y^*(t)$ in comparison with the estimated lower and upper bounds resulting from the terminal current $i_T(t)$.
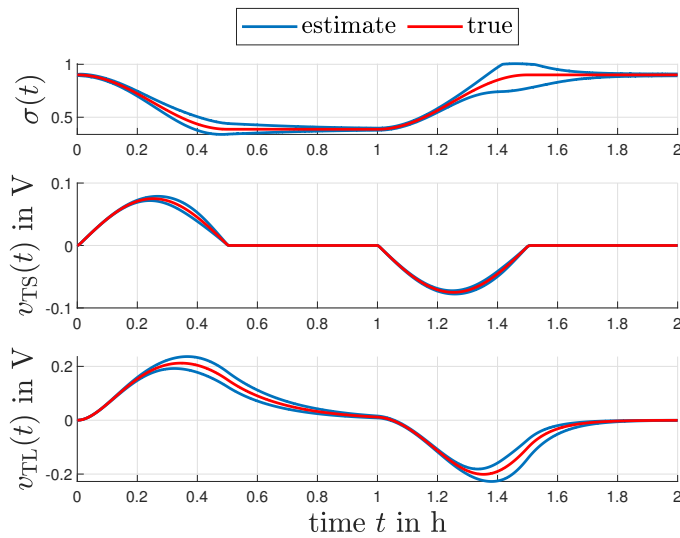

Figure 6: True value of the state variables in comparison with the estimated lower and upper bounds.
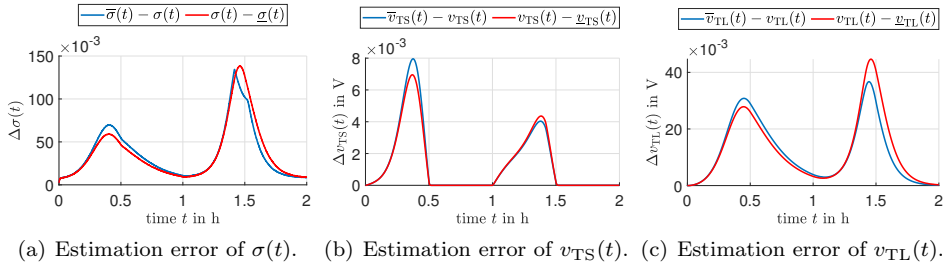
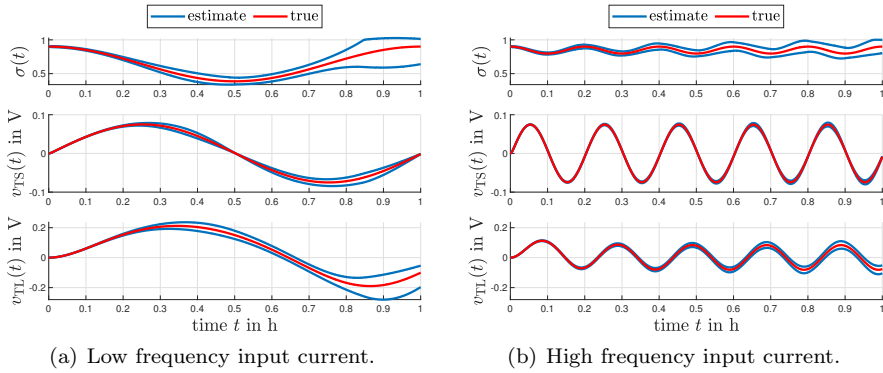(a) Estimation error of $\sigma(t)$.   (b) Estimation error of $v_{\mathrm{TS}}(t)$.   (c) Estimation error of $v_{\mathrm{TL}}(t)$.

Figure 7: Estimation errors of the state variables.

(a) Low frequency input current.   (b) High frequency input current.

Figure 8: Comparison of the estimated state variables resulting from low or high frequency input currents.

(a) Interval diameters of $\sigma(t)$. (b) Interval diameters of $v_{\mathrm{TS}}(t)$. (c) Interval diameters of $v_{\mathrm{TL}}(t)$.
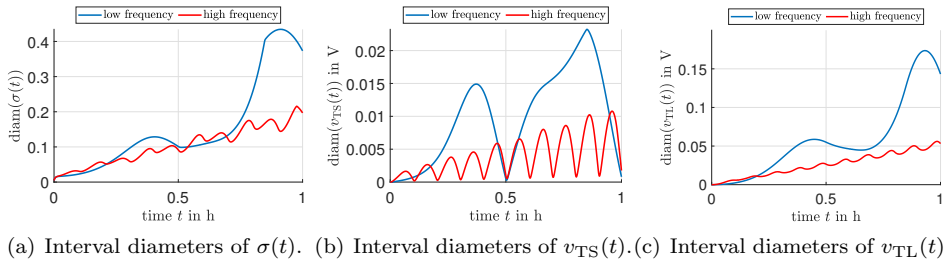
Figure 9: Comparison of the interval diameters of the estimated state variables resulting from the input currents according to Fig. 8.

(a) Discharge process (first sine half-wave).   (b) Charge process (second sine half-wave).
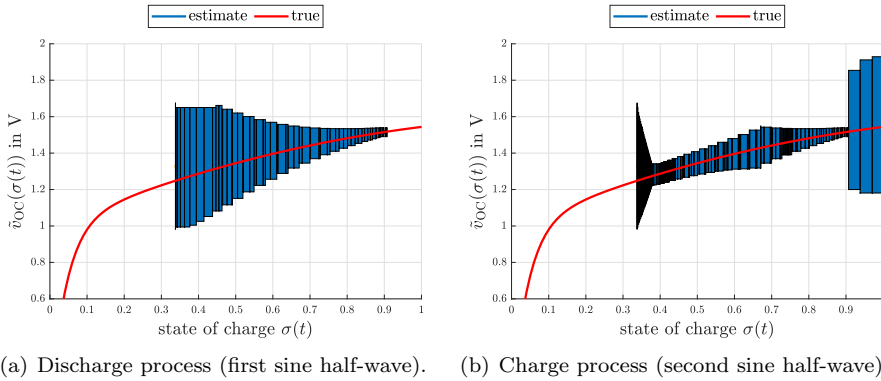
Figure 10: Approximation of the $v_{\mathrm{OC}}(\sigma(t))$ characteristic.

observer, afterwards the estimated values are used to correct an a-priori knowledge for the characteristic to be identified. The proposed identification routine was successfully applied to the identification of the open-circuit voltage characteristic of a lithium-ion battery.

The estimation quality has a major influence on the identification results. It is therefore necessary to reduce the estimation uncertainty as much as possible. As shown above, the input current strongly affects the estimation quality. So the design of optimal experiments by tuning the input current is very important. Furthermore, the design of the interval observer can be optimized to improve the estimation results. For example, a cascaded observer design or a TNL observer design as shown in [18] could be investigated.

In addition, our future work will deal with the extension of this approach to the identification of characteristics that depend on multiple variables (e.g. the open-circuit voltage characteristic of lithium-ion batteries that depends on the SOC and the temperature) and with the investigation of possible combinations of set-valued and stochastic approaches (cf. [11]).

References

[1] Barai, A., Uddin, K., Widanage, W. D., McGordon, A., and Jennings, P. A study of the influence of measurement timescale on internal resistance characterisation methodologies for lithium-ion cells. *Scientific Reports*, 8(1):21, 2018. DOI: 10.1038/s41598-017-18424-5.

[2] dit Sandretto, J. A., Trombettoni, G., Daney, D., and Chabert, G. Certified calibration of a cable-driven robot using interval contractor programming. In Thomas, F., editor, *Computational Kinematics*, Volume 15 of *Mechanisms and Machine Science Series*, pages 209–217. Springer Netherlands, Dordrecht, 2014. DOI: 10.1007/978-94-007-7214-4_24.

[3] Edge, J. S., O'Kane, S., Prosser, R., Kirkaldy, N. D., Patel, A. N., Hales, A., Ghosh, A., Ai, W., Chen, J., Yang, J., Li, S., Pang, M.-C., Bravo Diaz, L., Tomaszewska, A., Marzook, M. W., Radhakrishnan, K. N., Wang, H., Patel, Y., Wu, B., and Offer, G. J. Lithium ion battery degradation: What you need to know. *Physical Chemistry Chemical Physics (PCCP)*, 23(14):8200–8221, 2021. DOI: `10.1039/d1cp00359c`.

[4] Erdinç, O., Vural, B., and Uzunoğlu, M. A dynamic lithium-ion battery model considering the effects of temperature and capacity fading. In *Proceedings of International Conference on Clean Electrical Power (ICCEP)*, pages 383–386. IEEE, 2009. DOI: `10.1109/ICCEP.2009.5212025`.

[5] Gennat, M. and Tibken, B. Guaranteed bounds for uncertain systems: Methods using linear Lyapunov-like functions, differential inequalities and a midpoint method. In *Proceedings of the 12th GAMM — IMACS International Symposium on Scientific Computing, Computer Arithmetic and Validated Numerics (SCAN)*, page 17. IEEE, 2006. DOI: `10.1109/SCAN.2006.21`.

[6] Gennat, M. and Tibken, B. Computing guaranteed bounds for uncertain cooperative and monotone nonlinear systems. In *Proceedings of the 17th IFAC World Congress*, pages 4846–4851. IFAC Proceedings Volumes, 2008. DOI: `10.3182/20080706-5-KR-1001.00814`.

[7] Hildebrandt, E., Kersten, J., Rauh, A., and Aschemann, H. Robust interval observer design for fractional-order models with applications to state estimation of batteries. In *Proceedings of the 21st IFAC World Congress*, pages 3683–3688. IFAC-PapersOnLine, 2020. DOI: `10.1016/j.ifacol.2020.12.2052`.

[8] Jaulin, L. Robust set-membership state estimation; application to underwater robotics. *Automatica*, 45(1):202–206, 2009. DOI: `10.1016/j.automatica.2008.06.013`.

[9] Kersten, J., Rauh, A., and Aschemann, H. Transformation of uncertain linear fractional order differential equations into a cooperative form. In *Proceedings of the 11th IFAC Symposium on Nonlinear Control Systems (NOLCOS)*, pages 646–651. IFAC-PapersOnLine, 2019. DOI: `10.1016/j.ifacol.2019.12.035`.

[10] Krasnochtanova, I., Rauh, A., Kletting, M., Aschemann, H., Hofer, E. P., and Schoop, K.-M. Interval methods as a simulation tool for the dynamics of biological wastewater treatment processes with parameter uncertainties. *Applied Mathematical Modelling*, 34(3):744–762, 2010. DOI: `10.1016/j.apm.2009.06.019`.

[11] Lahme, M. and Rauh, A. Combination of stochastic state estimation with online identification of the open-circuit voltage of lithium-ion batteries. In *Proceedings of the 1st IFAC Workshop on Control of Complex Systems (COSY)*. IFAC-PapersOnLine, 2022. DOI: `10.1016/j.ifacol.2023.01.055`.

[12] Meddings, N., Heinrich, M., Overney, F., Lee, J.-S., Ruiz, V., Napolitano, E., Seitz, S., Hinds, G., Raccichini, R., Gaberšček, M., and Park, J. Application of electrochemical impedance spectroscopy to commercial Li-ion cells: A review. *Journal of Power Sources*, 480:228742, 2020. DOI: 10.1016/j.jpowsour.2020.228742.

[13] Middlemiss, L. A., Rennie, A. J., Sayers, R., and West, A. R. Characterisation of batteries by electrochemical impedance spectroscopy. In *Proceedings of the 4th Annual CDT Conference in Energy Storage & Its Applications*, pages 232–241. Energy Reports, 2019. DOI: 10.1016/j.egyr.2020.03.029.

[14] Raïssi, T. and Efimov, D. Some recent results on the design and implementation of interval observers for uncertain systems. *at - Automatisierungstechnik*, 66(3):213–224, 2018. DOI: 10.1515/auto-2017-0081.

[15] Rauh, A., Chevet, T., Dinh, T. N., Marzat, J., and Raïssi, T. Robust iterative learning observers based on a combination of stochastic estimation schemes and ellipsoidal calculus. In *Proceedings of the 25th International Conference on Information Fusion (FUSION)*, pages 1–8. IEEE, 2022. DOI: 10.23919/FUSION49751.2022.9841329.

[16] Rauh, A. and Kersten, J. Transformation of uncertain linear systems with real eigenvalues into cooperative form: The case of constant and time-varying bounded parameters. *Algorithms*, 14(3):85, 2021. DOI: 10.3390/a14030085.

[17] Reuter, J., Mank, E., Aschemann, H., and Rauh, A. Battery state observation and condition monitoring using online minimization. In *Proceedings of the 21st International Conference on Methods and Models in Automation and Robotics (MMAR)*, pages 1223–1228. IEEE, 2016. DOI: 10.1109/MMAR.2016.7575313.

[18] Wang, Z., Lim, C.-C., and Shen, Y. Interval observer design for uncertain discrete-time linear systems. *Systems & Control Letters*, 116:41–46, 2018. DOI: 10.1016/j.sysconle.2018.04.003.